Large intrinsic anomalous Hall effect in the hexagonal ferromagnet $NdCrGe_3$

Xiaojun Yang,* Junxiao Pan, and Dongliang Chu
College of Physics and Electronic Information, Luoyang Normal University, Luoyang 471022, China

(Received 23 December 2025; revised 5 March 2026; accepted 13 March 2026; published 27 March 2026)

We report the intrinsic anomalous Hall effect of $NdCrGe_3$ single crystals, which is a hexagonal ferromagnet metal with a one-dimensional crystal structure. The $NdCrGe_3$ undergoes multimagnetic transitions with a ferromagnetic transition at T_C~101 K and a spin reorientation transition at ~55 K. The Hall effect indicates that the dominant charge carriers shift from electrons to holes near T_C. Large anomalous Hall conductivity ~681.8 (600.3) Ω^{-1} cm^{-1} for $H//ab$ ($H//c$) is observed, consistent with the theoretically anticipated value derived from the intrinsic Berry-curvature mechanism. The linear scaling relationships observed between the anomalous Hall resistivity and the longitudinal resistivity offer strong and convincing evidence indicating that the intrinsic Karplus-Luttinger mechanism, rather than extrinsic side-jump and skew-scattering mechanisms, assumes a dominant position in the anomalous Hall effect. The distinctive crystal structure, unconventional complex magnetic interactions, and the observed intrinsic anomalous Hall effect could make $NdCrGe_3$ as a promising candidate for future electronic devices.

DOI: 10.1103/1mxv-fttm

I. INTRODUCTION

The anomalous Hall effect (AHE), marked by a sharp transverse voltage increase that arises when a longitudinal current flows through a magnetic material with spontaneous magnetization, stands as one of the most fundamental yet puzzling phenomena and has garnered widespread research interest from both the perspectives of fundamental physics and practical applications [1–5]. Three mechanisms that account for the AHE have gained broad recognition by researchers. The intrinsic Karplus-Luttinger (KL) mechanism, which is fundamentally and intricately tied to spin-orbit coupling, undergoes perturbation under the influence of an externally applied electric field, inducing the emergence of an extra term within the carrier group velocity [2,6]. In addition to other contributing factors, the AHE can also be generated through extrinsic mechanisms, specifically skew-scattering and side-jump mechanism, stemming from the asymmetric scattering behavior of conduction electrons [7–9]. The intrinsic mechanism linked to Berry curvature has garnered significant attention due to its remarkable ability to elucidate and forecast substantial AHE in topological materials, exemplified by compounds like RMn_6Sn_6 [10,11], Fe_3Sn_2 [12], and Co_2MnAl [13], and $Co_3Sn_2S_2$ [14,15], etc.

Exhibiting a wide array of intriguing and novel physical characteristics, the compounds $RCrGe_3$, where R represents rare earth elements La-Nd and Sm, adopt a hexagonal $BaNiO_3$-type crystal structure characterized by the space group $P6_3/mmc$ (No. 194) [16,17]. Materials that crystallize within the space group $P6_3/mmc$, encompassing notable examples such as the candidate ferromagnetic nodal-line semimetal Fe_3GeTe_2 [18,19], the topological superconductor $BaSn_3$ [20], and the Ising ferromagnet $FeCr_2Te_4$ [21,22], have recently become the focus of considerable attention, presumably due to their distinctive crystalline symmetry which imbues them with the potential to exhibit topological nontriviality, thereby making them highly promising candidates meriting both in-depth theoretical analysis and experimental investigation [19,20,23]. Diverse intriguing physical properties have been found in $RCrGe_3$ systems. In $LaCrGe_3$, the avoidance of a ferromagnetic (FM) quantum criticality has been comprehensively investigated under pressure [24,25], and large anomalous Hall conductivity dominated by intrinsic effects has been observed recently [26]. In $CeCrGe_3$, which is a ferromagnetic Kondo lattice with heavy fermion behaviors [27], strikingly large anomalous Hall and Nernst effects correlated to Berry curvature at the Fermi energy are detected [28]. For $PrCrGe_3$, we previously measured the critical behavior and magnetocaloric effect [29], and large anomalous Hall effect induced by skew scattering has been observed recently by Yu *et al.* [30]. Obviously, the origin of the large anomalous Hall effect in $RCrGe_3$ system is diverse and full of controversy. For $NdCrGe_3$, the magnetic measurements on a polycrystalline sample show ferromagnetic ordering at 122 K [17], then a neutron diffraction study reveals an axial ferromagnetic arrangement of both the Cr and Nd sublattices below $T_C \sim 122$ K [31]. We have investigated the multiple magnetic transitions in $NdCrGe_3$ single crystal with T_C~101 K by critical behavior and magnetocaloric effect [32]. Furthermore, comprehensive investigations have been carried out to examine the magnetic, magnetocaloric, and thermoelectric properties of the polycrystalline $NdCrGe_3$ sample with $T_C \sim 122$ K [33]. Additionally, competing magnetic states have been reported in $Nd_{1-x}La_xCrGe_3$ single crystals with the T_C of $NdCrGe_3 \sim 104$ K [34]. Some variance in the characteristic temperatures, i.e., $T_C \sim 122$ K in polycrystals and $T_C \sim 101$ K in single crystals, could be due to the fact that the single crystals were synthesized via a flux method that yields higher crystalline quality but minor compositional

*Contact author: xiaojunyang01@foxmail.com

fluctuations compared to the polycrystalline samples. Systematic investigations focusing on the electrical transport properties of $NdCrGe_3$ single crystals are still absent.

In this work, the heat capacity, magnetic, and electrical transport properties of $NdCrGe_3$ were comprehensively investigated. The $NdCrGe_3$ undergoes multimagnetic transitions with a ferromagnetic transition at $T_C \sim 101$ K and a spin reorientation of Cr moments at 55 K. The field-dependent MR and Hall effect are well in line with the isothermal magnetization curves. Large intrinsic AHC is observed, reaching $\sim$681.8 (600.3) Ω^{-1} cm^{-1} for $H//ab$ ($H//c$). The linear scaling curves of σ_{xy}^A vs M_s and $\rho_{yx}/\mu_0 H_{\mathrm{eff}}$ vs $\rho_{xx}^2 M/\mu_0 H_{\mathrm{eff}}$ demonstrate the AHE is predominantly governed by the contribution arising from the intrinsic Berry-phase-related KL mechanism.

II. EXPERIMENTAL DETAILS

The details regarding single-crystal growth and its crystal structure are presented in our previous reports [32]. An optical image of a typical crystal is presented in the (ii) inset of Fig. 1(b). The crystal orientations are displayed in the (iii) inset of Fig. 1(b). When the field is along y (z) direction, it is marked as ($H//ab$) $H//c$ in the context. The magnetization was measured in quantum design magnetic property measurement system MPMS-XL7. The specific heat and electrical transport were measured in the quantum design physical property measurement system (PPMS-9). The measurements of longitudinal and Hall resistivity were carried out utilizing the standard four-probe technique. The samples were polished to rectangular bar to attach four contacts. The size of the investigated samples is $1.5 \times 0.67 \times 0.35$ mm^3 for $H//ab$ plane and $0.67 \times 0.35 \times 0.25$ mm^3 for $H//c$ axis. The measured crystals for magnetization, specific heat, and transport properties are from the same batch of synthesis. To remove the effect of probe misalignment, Hall resistivity and longitudinal resistivity were antisymmetrized and symmetrized, respectively, i.e., $\rho_{yx}(H) = [\rho_{yx}(+H) - \rho_{yx}(-H)]/2$ and $\rho_{xx}(H) = [\rho_{xx}(+H) + \rho_{xx}(-H)]/2$. The applied magnetic field H_a is corrected to the internal field as $H_i = H_a - N_d M$, where M and N_d are the magnetization and the demagnetization factor, respectively. The corrected field H_i was used for the analyses.

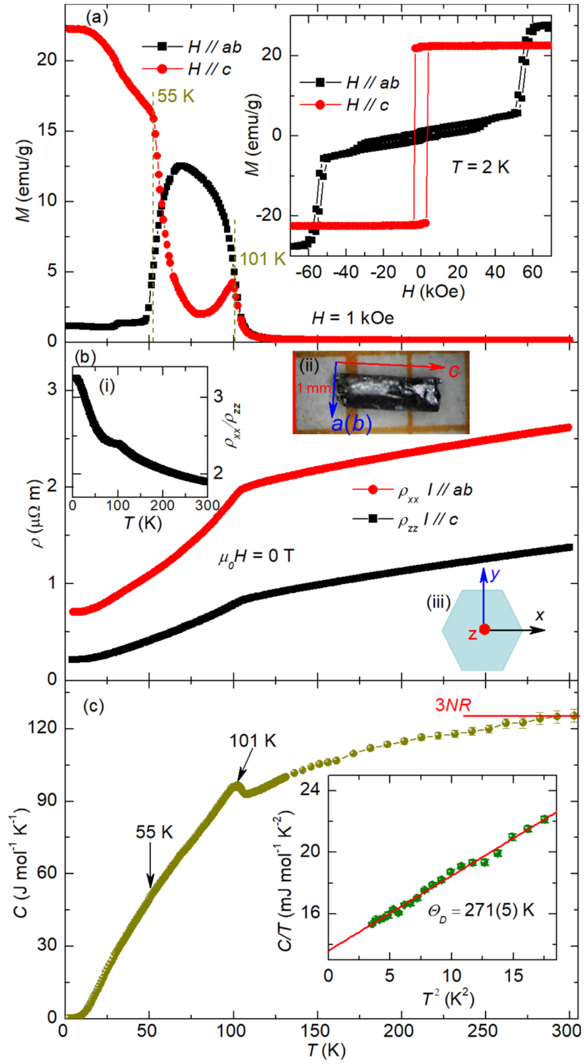

FIG. 1. (a) Temperature dependence of magnetization curves of $NdCrGe_3$ under 1 kOe. Inset: Isothermal magnetization curves at $T = 2$ K. (b) Temperature dependence of in-plane resistivity ρ_{xx} and out-of-plane resistivity ρ_{zz}. Inset: (i) ρ_{xx}/ρ_{zz} versus temperature T, (ii) an optical image of a typical crystal, (iii) the crystal orientations. (c) Temperature-dependent heat capacity $C_p(T)$. Inset: $C_p(T)/T$ vs T^2 in low temperatures with a linear fitting curve.

III. RESULTS AND DISCUSSION

The magnetization curves as a function of a temperature of $NdCrGe_3$ under $H = 1$ kOe for $H//ab$ and $H//c$ are displayed in Fig. 1(a), where strong anisotropic magnetic properties with two main magnetic transitions at $T \sim 101$ and 55 K are observed, consistent with the previously detected a paramagnetic (PM)-FM transition at 101 K and a spin reorientation at 55 K [32]. The large anisotropic effect is also manifested by the field-dependent isothermal magnetization curves at $T = 2$ K [inset of Fig. 1(a)]. The magnetic properties are in good agreement with our previous reports [32]. The anisotropic behavior is also present in resistivity with a large $\rho_{xx}/\rho_{zz} = 3.3$ at 2 K [inset (i) of Fig. 1(b)]. The temperature dependence of resistivity $\rho(T)$ under zero field for $I//ab$ plane and $I//c$ axis exhibit metallic behaviors with relatively low residual-resistivity-ratios of 3.8 and 6.3 for $I//ab$ and $I//c$, respectively [Fig. 1(b)]. The kinks at $\sim$101 K is consistent with the magnetic transition at T_C. The temperature-dependent heat capacity $C_p(T)$ for $NdCrGe_3$ is presented in Fig. 1(c), where a clear λ-type transition at 101 K and a small anomaly at 55 K can be observed, agreeing well with the transitions in $M(T)$ curves. The $C_p(T)$ at high temperature ($\geqslant$275 K) matches well with the Dulong Petit value $3NR = 124.7$ J mol^{-1} K^{-1}, where $N = 5$ is the number of atoms per formula unit and $R = 8.314$ J mol^{-1} K^{-1} is the molar gas constant. The low-temperature data of heat capacity can be well fitted by $C_p(T)/T = \gamma + \beta T^2$ [inset of Fig. 1(c)], where γ and β represent the Sommerfeld electronic specific-heat coefficient and the lattice heat capacity coefficient in low-temperature limit, respectively. The fitting yields the following results: $\gamma = 13.6$ mJ mol^{-1} K^{-2} and $\beta = 0.487$ mJ mol^{-1} K^{-4}. With the equation $\Theta_D =$

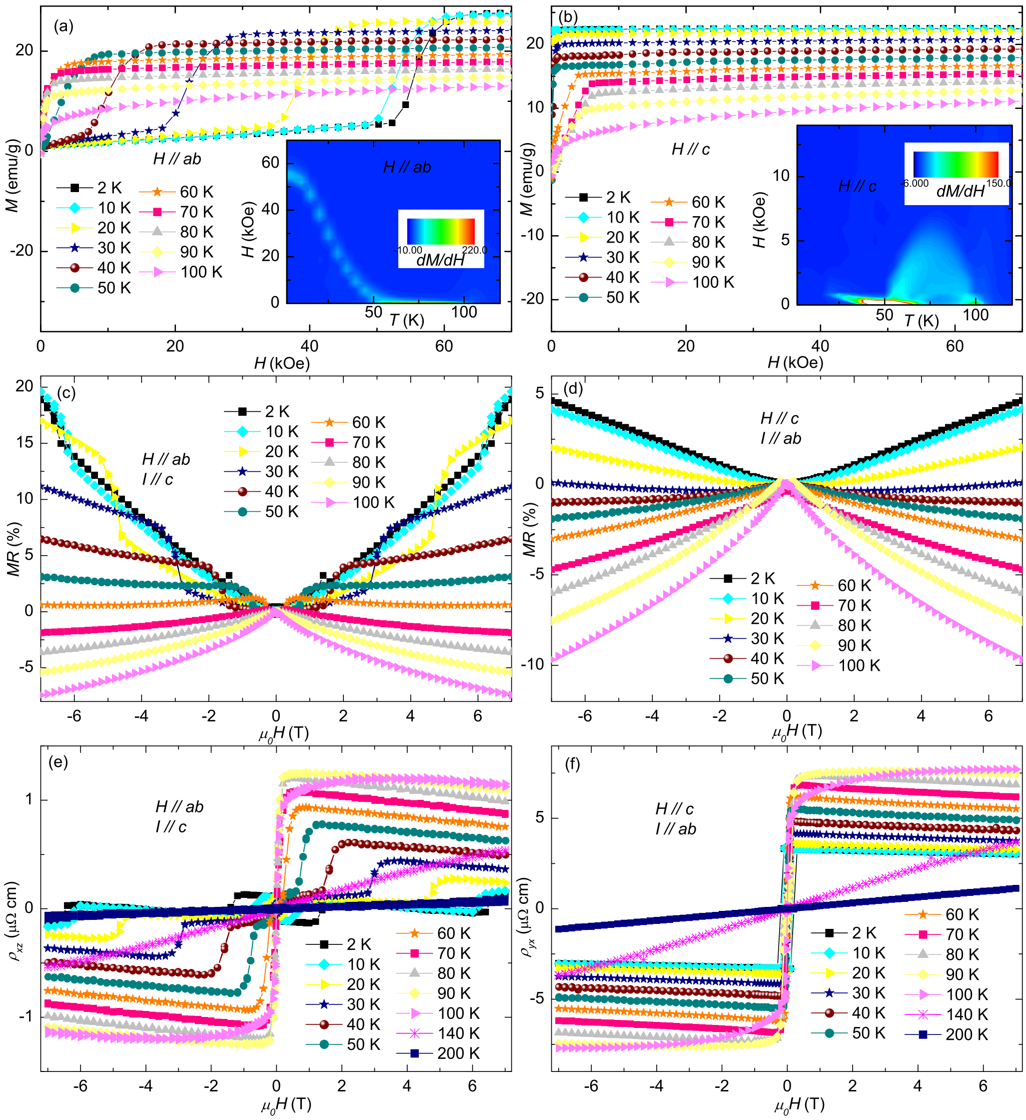

FIG. 2. (a), (b) Isothermal magnetization curves for (a) $H//ab$ and (b) $H//c$ at different temperatures. Insets: the contour plots of dM/dH, displaying the M-H phase diagram. (c), (d) The magnetoresistance (MR) versus field H for $NdCrGe_3$ at various temperatures with (c) $H//ab$ and (d) $H//c$. (e), (f) The field-dependent Hall resistivity under (e) $H//ab$ and (f) $H//c$.

$(12\pi^4 NR/5\beta)^{1/3}$, the Debye temperature $\Theta_D = 271(5)$ K can be acquired.

Figures 2(a) and 2(b) show the plots of $M(H)$ curves at various temperatures for $H//ab$ and $H//c$. When $T < T_C$, the $M(H)$ curves exhibits a rapid rise at low magnetic fields and reaches saturation in the high-magnetic-field region, demonstrating characteristics typical of ferromagnets. Below the transition around $T = 55$ K, metamagnetic transitions can be found in the $M(H)$ curves of $H//ab$, which could be due to the reorientation of Cr moments, consistent with previous literature [32]. With the detailed measured $M(H)$ curves, the field and temperature dependence of derivative magnetization (dM/dH) can be evaluated, resulting in the contour plots in the insets of Figs. 2(a) and 2(b), which clearly distinguish the critical fields of the magnetic transitions at 55 and 101 K and map out the phase diagram for the complex magnetic interactions. As reported by Lemoine *et al.* via neutron diffraction [31], $NdCrGe_3$ exhibits a complex magnetic structure where Cr and Nd moments order ferromagnetically at high temperature ~122 K, and Nd moments undergo a subsequent ordering transition at low temperature ~70 K. The coupling between Cr and Nd sublattices is nonnegligible: the two magnetic sublattices are ordered separately, but at the same time the Cr sublattice, which orders at a higher temperature, polarizes the Nd sublattice. For our results on magnetic and magnetotransport, the metamagnetic transition observed in $H//ab$ below 55 K may be associated with the reorientation of Cr moments, which result from the interplay between Cr sublattice reordering and Nd moment alignment, consistent with the phase boundary features noted in the dM/dH inset. We also compared our characteristic temperature (e.g., the ~101 K transition) with the report of transition at ~122 K [31,33], attributing the slight discrepancy to sample-dependent variations in stoichiometry, as our single crystals were synthesized via a flux method that yields higher crystalline quality but minor compositional fluctuations compared to the polycrystalline samples used in some previous studies. Other results on the single crystalline sample with characteristic temperatures $T_C \sim 104$ K are compatible with our data within experimental error [34].

The magnetoresistance (MR $= [\rho(\mu_0 H) - \rho(0)]/\rho(0) \times 100\%$) as a function of fields for $H//ab$ and $H//c$ are displayed in Figs. 2(c) and 2(d), both of which exhibit complex competitive behavior. Below 60 (30) K for $H//ab$ ($H//c$), the MR is positive and shows a consistent monotonically increasing trend as the magnetic field intensifies. This phenomenon can be ascribed to the Lorentz force, generated by the applied magnetic field, which impedes the motion of charge carriers [35,36]. The positive MR exhibits a gradual increase as the temperature decreases, which can be attributed to the fact that the influence of the Lorentz force on MR becomes progressively more significant with the lowering of temperature. For $H//ab$, sharp transitions can be observed below 55 K, which agrees well with the metamagnetic transitions in $M(H)$ curves. Above 60 (30) K for $H//ab$ ($H//c$), the MR manifests as negative and demonstrates a nonmonotonic variation with increasing temperature, a characteristic commonly observed in ferromagnetic metals; this negative MR arises from the magnetic field's suppression of electron-magnon scattering processes [37].

Field dependence of the Hall resistivity for $H//ab$ (ρ_{xz}) and $H//c$ (ρ_{yx}) is displayed in Figs. 2(e) and 2(f), respectively. Below 50 K, the variation of ρ_{xz} are well consistent with the $M(H)$ curves with two step transitions probably due to metamagnetic transition for $H//ab$. For $H//ab$, the metamagnetic transitions in the MR and Hall data [Figs. 2(c) and 2(e)] are at higher fields than for the magnetization data [Fig. 2(a)]. Since the misalignment the effect between the *ab* plane and *c* axis can never be totally corrected in an anisotropic system, and metamagnetic transitions only occur in the $H//ab$ plane, a higher magnetic field should be applied to reach the transition field when there is a slight misalignment of the magnetic field with respect to the *c* axis. This can lead to different metamagnetic transition fields between Hall and magnetization measurements. The above conclusion is further supported by the well-matched metamagnetic transition fields of MR and Hall, as MR and Hall are measured simultaneously using a Hall bar. As the difference of saturated magnetization for $H//ab$ and $H//c$ is not very large (e.g., $\sim$13.6% at 80 K), and the analysis on Hall effect is only corresponding to the high-field data, a slight misalignment like $\sim$10% will not have a large effect on the resulting analysis on Hall effect. In the temperature range of 60–100 K for $H//ab$ (ρ_{xz}) and 2–100 K for $H//c$ (ρ_{yx}) below T_C, the Hall resistivity undergoes a sharp and significant increase, and this phenomenon is a clear sign of the presence of an anomalous Hall response. The saturation magnetization of $\sim$27.6 emu/g (or 2.05 μ_B/f.u.) for $H//ab$ and 22.5 emu/g (or 1.67 μ_B/f.u.) for $H//c$ at 2 K is lower than the expected value if both Nd and Cr moments are fully ferromagnetically aligned ($\sim$1 μ_B/f.u. for Cr^{3+} [31,32] and $\sim$3.6 μ_B/f.u. for Nd^{3+}). This discrepancy, as discussed in our previous work [32], arises from the coexistence of ferromagnetic and other complex magnetic interactions in $NdCrGe_3$. For the Hall effect analysis, the AHE is sensitive to the net

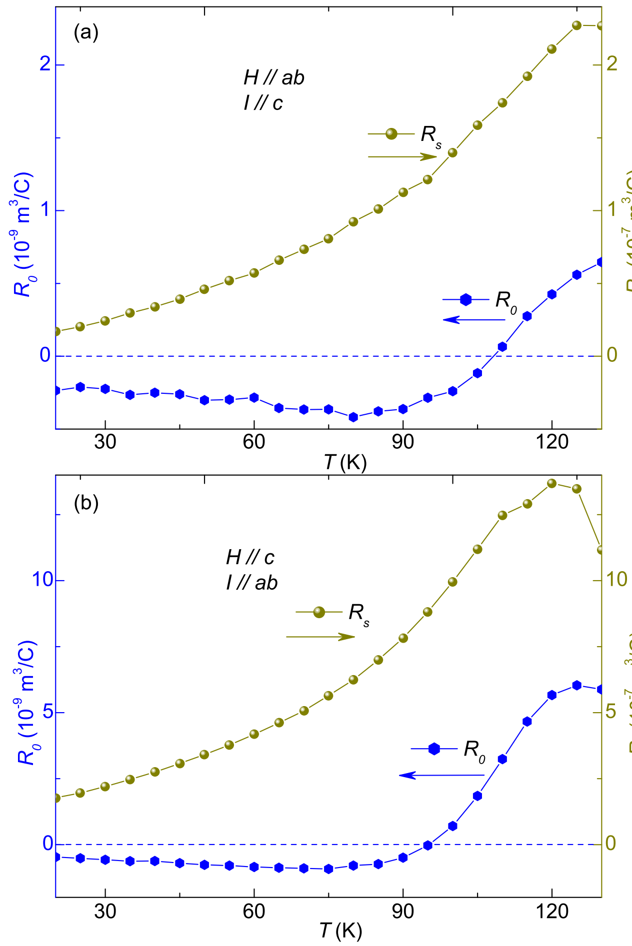

FIG. 3. Temperature dependence of the normal and anomalous Hall coefficient R_0 (left axis) and R_s (right axis) for (a) $H//ab$ (ρ_{xz}) and (b) $H//c$ (ρ_{yx}).

magnetization, so the reduced saturation magnetization means the AHE contribution is weaker than in a fully ferromagnetic system. Synoradzki *et al*. show a further increase in magnetization at 2 K beyond 8 T [33], further experiments extending the magnetic field range above 8 T are worthy of being carried out in future work. the further increase in magnetization could be due to the same origin of the metamagnetic transition with different critical fields in polycrystalline and single crystalline samples.

In ferromagnets, the Hall resistivity ρ_{yx} generally consists of two parts [1,30,38],

$$\rho_{yx} = \rho_{yx}^O + \rho_{yx}^A = R_0 B + R_s \mu_0 M, \tag{1}$$

where ρ_{yx}^O is the ordinary Hall resistivity and ρ_{yx}^A is anomalous Hall resistivity, and R_0 represents the ordinary Hall coefficient and R_s denotes the anomalous Hall coefficient. Well below T_C, the R_0 and ρ_{yx}^A, which can be determined by a linear fit to the ρ_{yx} vs B curve in the high-field region, are the slope and intercept of *y*axis, respectively. Around T_C, the large change in M prevents accurate determination of the coefficients by the above linear fitting. We fit the coefficients around T_C using a linear fit to the ρ_{yx}/B vs $\mu_0 M/B$ curves in high field

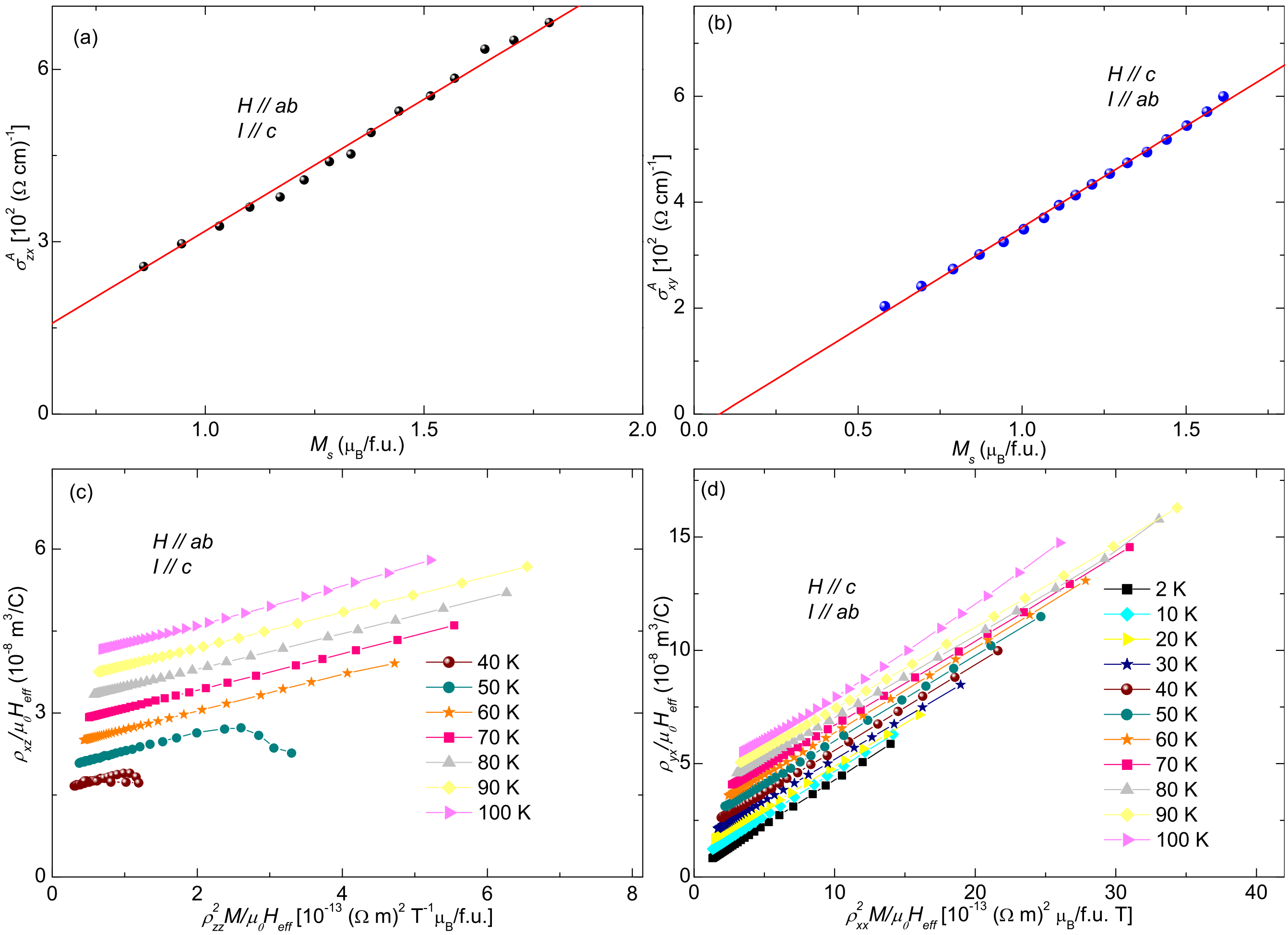

FIG. 4. (a), (b) The anomalous Hall conductivity σ_{xy}^A as a function of magnetization (M_s) for (a) $H//ab$ (σ_{zx}^A) (b) $H//c$ (σ_{xy}^A). (c), (d). The scaling plots of $\rho_{yx}/\mu_0 H_{\text{eff}}$ versus $\rho_{xx}^2 M/\mu_0 H_{\text{eff}}$ curves at several temperatures with vertically shifts of 4×10^{-9} m^3 C^{-1} for clarity for (c) $H//ab$ and (d) $H//c$.

region (Fig. S1 in Supplemental Material [39]), because the equation $\rho_{yx}/B = R_0 + R_s \mu_0 M/B$ considers the curvature of $M(H)$ curves around T_C. As displayed in the left axis of Fig. 3, the R_0 changes from positive to negative at $\sim T_C$ with a decreasing of the temperature, demonstrating the majority electronic carriers alternate from hole type to electronic type, which could be associated with the Lifshitz transition or the temperature-dependent variation in carrier mobilities and band occupations [30,40,41]. Furthermore, the R_s [right axis of Fig. 3] can be acquired by the equation $\rho_{yx}^A = R_s \mu_0 M_s$, where M_s is obtained by a linear fit to the plots of M vs H at the high-field regime, which is positive in the whole temperature region. In addition, the value of R_s exceeds that of R_0 by two orders of magnitude, indicating the Hall resistivity is dominated by the anomalous part. The carrier concentration can be estimated $n \sim 10^{28}$ m^{-3}, combining with the resistivity of 1~2 μΩ m [Fig. 1(b)] around T_c, a mean free path (λ) of about 10 Å can be evaluated, which is comparable with the lattice constants and close to the Mott-Ioffe-Regel limit [38,42], indicating a metallic behavior in dirty region.

Three potential mechanisms have been proposed to account for the AHE. Recently, the intrinsic KL mechanism has undergone a reinterpretation, highlighting a Berry curvature term [43,44]. This term represents an inherent characteristic of the occupied electronic states within a crystal possessing specific symmetry. It takes on a nonzero value under two specific conditions: either the time-reversal symmetry is broken or there exists a net magnetic moment. The intrinsic mechanism gives rise to a quadratic scaling relationship expressed as $\rho_{yx}^A = \beta \rho_{xx}^2$. The side-jump mechanism is one where the potential field generated by impurities plays a part in creating an anomalous group velocity. Interestingly, it demonstrates the same quadratic scaling pattern as the KL mechanism. On the other hand, the skew-scattering mechanism, which is responsible for asymmetric scattering due to impurities or defects, can also make a contribution to the AHE. It shows a distinct linear scaling behavior, namely $\rho_{yx}^A = \beta \rho_{xx}$.

In theory, the the magnitude of the intrinsic anomalous Hall conductivity $\sigma_{xy,\text{in}}^A$ $(=\rho_{yx}^A/(\rho_{xx}^2 + \rho_{yx}^2) \sim \rho_{yx}^A/\rho_{xx}^2)$ is shown to be on the order of $e^2/(ha)$, where a is the lattice constant, h is the Plank constant, and e is the charge constant [2,38]. Taking $a = V^{1/3} \sim 5.7$ Å approximately for the $NdCrGe_3$ sample, the estimated $\sigma_{xy,\text{in}}^A \sim 678$ Ω^{-1} cm^{-1}, which is the same magnitude of order of the experimentally measured AHE as shown in Figs. 4(a) and 4(b), with large AHC reaching up to ~681.8 (600.3) Ω^{-1} cm^{-1} for $H//ab$ ($H//c$). In contrast, it has been demonstrated that the extrinsic side-jump contribution to $\sigma^A_{xy,sj}$ is on the order of $e^2/(ha)\varepsilon_{SO}E_F$, where E_F denotes the Fermi energy and ε_{SO} represents the spin-orbit interaction strength [45], which can be comparable with the value of $e^2/(ha)$ only in the ultraclean limit [46,47]. In metallic ferromagnets, the product $\varepsilon_{SO}E_F$ usually remains below 0.01, the extrinsic side-jump effect is expected to be much smaller than the experimentally obtained value, indicating the AHE in $NdCrGe_3$ is predominantly governed by the intrinsic KL contribution. Furthermore, the intrinsic anomalous Hall conductivity is in proportion to magnetization M [3], which is indeed observed in Figs. 4(a) and 4(b), exhibiting linear fits with scaling coefficient $S_H = \sigma^A_{xy}/M = 0.46(3)$ and 0.38(2) V^{-1} for $H//ab$ and $H//c$, the value is larger than those traditional metallic ferromagnets, such as Ni and Fe ($S_H \sim 0.01$–$0.2\ V^{-1}$) [48,49]. The intercepts in Figs. 4(a) and 4(b) are not zero, which is further indicative of a complex magnetic structure and is consistent with previous publications on magnetization [32]. Furthermore, Figs. 4(c) and 4(d) displays the scaling plots of the modified anomalous Hall resistivity versus modified longitudinal resistivity ($\rho_{xz}/\mu_0 H_{eff}$ vs $\rho^2_{zz}M/\mu_0 H_{eff}$ for $H//ab$ and $\rho_{yx}/\mu_0 H_{eff}$ vs $\rho^2_{xx}M/\mu_0 H_{eff}$ for $H//c$) at several temperatures. To enhance clarity, the scaling curves have been vertically shifted by $4 \times 10^{-9}\ m^3\ C^{-1}$. Without offset all the curves collapse onto one universal curve (Fig. S2 [39]). In Figs. 4(a) and 4(b), the temperature is an implicit parameter, while in Figs. 4(c) and 4(d), H is the implicit parameter for each curve. This indicates that the quadratic scaling relationship $\rho^A_{yx} = \beta\rho^2_{xx}$ is suitable for the $NdCrGe_3$ sample, regardless of whether temperature or magnetic field is varied. The linear behavior that remains consistent across a range of different temperatures offers additional corroborative evidence, reinforcing the conclusion that the AHE in $NdCrGe_3$ is best characterized by the intrinsic KL theory.

IV. CONCLUSIONS

To summarize, a comprehensive investigation has been carried out on the electrical transport properties of the $NdCrGe_3$ single crystal. The sign of MR undergoes a transition from positive to negative in the vicinity of 60 (30) K for $H//ab$ ($H//c$) as the temperature increases, resulting from the competition between the increased scattering by Lorentz force and the suppression of electron-magnon scattering. The measured Hall effect indicates the dominating carriers change from negative to positive at around $T_C \sim 101$ K. The large AHC reaches up to ∼681.8 (600.3) $\Omega^{-1}\ cm^{-1}$ for $H//ab$ ($H//c$), the value aligns with the contribution stemming from the intrinsic Berry curvature. The linear scaling behavior indicates that the intrinsic KL mechanism plays a predominant role in the observed AHE. With the swift advancement of low-dimensional materials in the field of spintronics, there is significant interest in conducting further research on the AHE within the nanosheet structure of $NdCrGe_3$.

ACKNOWLEDGMENTS

The work is supported by the National Natural Science Foundation of China (Grant No. 12404136) and the Natural Science Foundation of Henan Province (Grant No. 242300421692).

DATA AVAILABILITY

The data that support the findings of this article are not publicly available upon publication because it is not technically feasible and/or the cost of preparing, depositing, and hosting the data would be prohibitive within the terms of this research project. The data are available from the authors upon reasonable request.

[1] N. Nagaosa, J. Sinova, S. Onoda, A. H. MacDonald, and N. P. Ong, Anomalous Hall effect, Rev. Mod. Phys. **82**, 1539 (2010).
[2] S. Onoda, N. Sugimoto, and N. Nagaosa, Intrinsic versus extrinsic anomalous Hall effect in ferromagnets, Phys. Rev. Lett. **97**, 126602 (2006).
[3] N. Manyala, Y. Sidis, J. F. Ditusa, G. Aeppli, D. P. Young, and Z. Fisk, Large anomalous Hall effect in a silicon-based magnetic semiconductor, Nat. Mater. **3**, 255 (2004).
[4] O. K. Forslund, X. Liu, S. Shin, C. Lin, M. Horio, Q. Wang, K. Kramer, S. Mukherjee, T. Kim, C. Cacho, C. Wang, T. Shang, V. Ukleev, J. S. White, P. Puphal, Y. Sassa, E. Pomjakushina, T. Neupert, and J. Chang, Anomalous Hall effect due to magnetic fluctuations in a ferromagnetic Weyl semimetal, Phys. Rev. Lett. **134**, 126602 (2025).
[5] J. Chen, X. Yang, F. Zhou, Y. C. Lau, W. Feng, Y. Yao, Y. Li, Y. Jiang, and W. Wang, Colossal anomalous Hall effect in the layered antiferromagnetic $EuAl_2Si_2$ compound, Mater. Horiz. **11**, 4665 (2024).
[6] R. Karplus and J. M. Luttinger, Hall effect in ferromagnetics, Phys. Rev. **95**, 1154 (1954).
[7] J. Smit, The spontaneous Hall effect in ferromagnetics I, Physica **21**, 877 (1955).
[8] J. Smit, The spontaneous Hall effect in ferromagnetics II, Physica **24**, 39 (1958).
[9] L. Berger, Side-jump mechanism for the Hall effect of ferromagnets, Phys. Rev. B **2**, 4559 (1970).
[10] J. X. Yin, W. L. Ma, T. A. Cochran, X. T. Xu, S. T. S. Zhang, H. J. Tien, N. Shumiya, G. M. Cheng, K. Jiang, B. Lian, Z. D. Song, G. Q. Chang, I. Belopolski, D. Multer, M. Litskevich, Z. J. Cheng, X. P. Yang, B. Swidler, H. B. Zhou, *et al.*, Quantum-limit Chern topological magnetism in $TbMn_6Sn_6$, Nature (London) **583**, 533 (2020).
[11] W. L. Ma, X. T. Xu, J. X. Yin, H. Yang, H. B. Zhou, Z. J. Cheng, Y. Q. Huang, Z. Qu, F. Wang, M. Z. Hasan, and S. Jia, Rare earth engineering in RMn_6Sn_6 (R = Gd-Tm, Lu) topological kagome magnets, Phys. Rev. Lett. **126**, 246602 (2021).
[12] L. Ye, M. Kang, J. Liu, F. von Cube, C. R. Wicker, T. Suzuki, C. Jozwiak, A. Bostwick, E. Rotenberg, D. C. Bell, L. Fu, R. Comin, and J. G. Checkelsky, Massive Dirac fermions in a ferromagnetic kagome metal, Nature (London) **555**, 638 (2018).
[13] P. Li, J. Koo, W. Ning, J. Li, L. Miao, L. Min, Y. Zhu, Y. Wang, N. Alem, C. X. Liu, Z. Mao, and B. Yan, Giant room temperature anomalous Hall effect and tunable topology in a

ferromagnetic topological semimetal Co_2MnAl, Nat. Commun. **11**, 3476 (2020).

[14] E. Liu, Y. Sun, N. Kumar, L. Muechler, A. Sun, L. Jiao, S. Y. Yang, D. Liu, A. Liang, Q. Xu, J. Kroder, V. Süß, H. Borrmann, C. Shekhar, Z. Wang, C. Xi, W. Wang, W. Schnelle, S. Wirth, Y. Chen, *et al.*, Giant anomalous Hall effect in a ferromagnetic kagome-lattice semimetal, Nat. Phys. **14**, 1125 (2018).

[15] Q. Wang, Y. Xu, R. Lou, Z. Liu, M. Li, Y. Huang, D. Shen, H. Weng, S. Wang, and H. Lei, Large intrinsic anomalous Hall effect in half-metallic ferromagnet $Co_3Sn_2S_2$ with magnetic Weyl fermions, Nat. Commun. **9**, 3681 (2018).

[16] X. Lin, V. Taufour, S. L. Budko, and P. C. Canfield, Suppression of ferromagnetism in the $LaV_xCr_{1-x}Ge_3$ system, Phys. Rev. B **88**, 094405 (2013).

[17] H. Bie, O. Y. Zelinska, A. V. Tkachuk, and A. Mar, Structures and physical properties of rare-Earth chromium germanides $RECrGe_3$ (RE = La-Nd, Sm), Chem. Mater. **19**, 4613 (2007).

[18] Y. Deng, Y. Yu, Y. Song, J. Zhang, N. Z. Wang, Z. Sun, Y. Yi, Y. Z. Wu, S. Wu, J. Zhu, J. Wang, X. H. Chen, and Y. Zhang, Gate-tunable room-temperature ferromagnetism in two-dimensional Fe_3GeTe_2, Nature (London) **563**, 94 (2018).

[19] K. Kim, J. Seo, E. Lee, K.-T. Ko, B. S. Kim, B. G. Jang, J. M. Ok, J. Lee, Y. J. Jo, W. Kang, J. H. Shim, C. Kim, H. W. Yeom, B. I. Min, B.-J. Yang, and J. S. Kim, Large anomalous Hall current induced by topological nodal lines in a ferromagnetic van der waals semimetal, Nat. Mater. **17**, 794 (2018).

[20] K. Huang, A. Y. Luo, C. Chen, G. N. Zhang, X. L. Liu, Y. W. Li, F. Wu, S. T. Cui, Z. Sun, C. Jozwiak, A. Bostwick, E. Rotenberg, H. F. Yang, L. X. Yang, G. Xu, Y. F. Guo, Z. K. Liu, and Y. L. Chen, Observation of topological dirac fermions and surface states in superconducting $BaSn_3$, Phys. Rev. B **103**, 155148 (2021).

[21] Y. Liu, H. Tan, Z. Hu, B. Yan, and C. Petrovic, Anomalous Hall effect in the weak-itinerant ferrimagnet $FeCr_2Te_4$, Phys. Rev. B **103**, 045106 (2021).

[22] Y. Liu, R. J. Koch, Z. Hu, N. Aryal, E. Stavitski, X. Tong, K. Attenkofer, E. S. Bozin, W. Yin, and C. Petrovic, Three-dimensional Ising ferrimagnetism of Cr-Fe-Cr trimers in $FeCr_2Te_4$, Phys. Rev. B **102**, 085158 (2020).

[23] T. Zhang, Y. Jiang, Z. Song, H. Huang, Y. He, Z. Fang, H. Weng, and C. Fang, Catalogue of topological electronic materials, Nature (London) **566**, 475 (2019).

[24] V. Taufour, U. S. Kaluarachchi, R. Khasanov, M. C. Nguyen, Z. Guguchia, P. K. Biswas, P. Bonf, R. De Renzi, X. Lin, S. K. Kim, E. D. Mun, H. Kim, Y. Furukawa, C. Z. Wang, K. M. Ho, S. L. Bud, and P. C. Canfield, Ferromagnetic quantum critical point avoided by the appearance of another magnetic phase in $LaCrGe_3$ under pressure, Phys. Rev. Lett. **117**, 037207 (2016).

[25] U. S. Kaluarachchi, S. L. Bud, P. C. Canfield, and V. Taufour, Tricritical wings and modulated magnetic phases in $LaCrGe_3$ under pressure, Nat. Commun. **8**, 546 (2017).

[26] M. Sariket, N. Islam1, S. Shamim, and N. Kumar, Exploring the signature of two ferromagnetic states and goniopolarity in $LaCrGe_3$ through Hall effect, arXiv:2508.21508.

[27] D. Das, T. Gruner, H. Pfau, U. B. Paramanik, U. Burkhardt, C. Geibel, and Z. Hossain, Heavy fermion and Kondo lattice behavior in the itinerant ferromagnet $CeCrGe_3$, J. Phys.: Condens. Matter **26**, 106001 (2014).

[28] L. F. Li, S. Y. Guan, S. W. Chi, J. W. Li, X. X. Lin, G. Xu, and S. Jia, Giant anomalous Hall and Nernst effects in a heavy fermion ferromagnet, arXiv:2401.17624.

[29] X. Yang, J. Pan, S. Liu, M. Yang, L. Cao, D. Chu, and K. Sun, Critical behavior and anisotropic magnetocaloric effect of the quasi-one-dimensional hexagonal ferromagnet $PrCrGe_3$, Phys. Rev. B **103**, 104405 (2021).

[30] Z. Yu, H. You, X. Luo, Y. Han, R. Zhong, Q. Luo, H. Yang, H. Wu, C. Chen, C. Fang, W. Ren, and S. Ma, Large anomalous Hall effect induced by skew scattering in the hexagonal ferromagnet $PrCrGe_3$, Phys. Rev. B **111**, 125112 (2025).

[31] P. Lemoine, J. M. Cadogan, B. R. Slater, A. Mar, and M. Avdeev, Neutron diffraction study of $NdCrGe_3$, J. Magn. Magn. Mater. **325**, 135 (2013).

[32] X. Yang, J. Pan, Y. Shi, K. Sun, L. Cao, and W. Sun, Magnetic properties of the hexagonal ferromagnet $NdCrGe_3$ showing metamagnetic transition and negative magnetocaloric effect, J. Phys. Chem. C **125**, 23370 (2021).

[33] K. Synoradzki, A. Frąckowiak, D. Szewczyk, T. J. Bednarchuk, D. Das, and D. Kaczorowski, Magnetic, magnetocaloric and thermoelectric properties of $NdCrGe_3$, J. Alloys Compd. **967**, 171713 (2023).

[34] C. Li, H. Liang, Y. Wang, Y. Liu, N. Li, Y. Zhou, Q. Li, D. Wu, X. Luo, N. Zhou, X. Sun, and Y. Sun, Competing magnetic states in quasi-one-dimensional hexagonal ferromagnetic $Nd_{1-x}La_xCrGe_3$ crystals, Appl. Phys. Lett. **126**, 212407 (2025).

[35] M. Singh, J. Sau, B. Rai, A. Panda, M. Kumar, and N. Kumar, Tuning intrinsic anomalous Hall effect from large to zero in two ferromagnetic states of $SmMn_2Ge_2$, Phys. Rev. Mater. **8**, 084201 (2024).

[36] T. Liang, Q. Gibson, M. N. Ali, M. Liu, R. J. Cava, and N. P. Ong, Ultrahigh mobility and giant magnetoresistance in the dirac semimetal Cd_3As_2, Nat. Mater. **14**, 280 (2015).

[37] J. Zhao, B. Jiang, S. Zhang, L. Wang, E. Liu, Z. Li, and X. Wu, Magnetoresistance signature of two-dimensional electronic states in $Co_3Sn_2S_2$, Phys. Rev. B **107**, 085203 (2023).

[38] Y. Liu, E. Stavitski, K. Attenkofer, and C. Petrovic, Anomalous Hall effect in the van der Waals bonded ferromagnet $Fe_{3-x}GeTe_2$, Phys. Rev. B **97**, 165415 (2018).

[39] See Supplemental Material at http://link.aps.org/supplemental/10.1103/1mxv-fttm for the plot of ρ_{yx}/B vs $\mu_0 M/B$ at $T = 100$ K for $H//c$ (Fig. S1) and the scaling plots of $\rho_{yx}/\mu_0 H_{\mathrm{eff}}$ vs $\rho_{xx}^2 M/\mu_0 H_{\mathrm{eff}}$ curves at several temperatures without offset (Fig. S2).

[40] F. C. Chen, Y. Fei, S. J. Li, Q. Wang, X. Luo, J. Yan, W. J. Lu, P. Tong, W. H. Song, X. B. Zhu, L. Zhang, H. B. Zhou, F. W. Zheng, P. Zhang, A. L. Lichtenstein, M. I. Katsnelson, Y. Yin, N. Hao, and Y. P. Sun, Temperature-induced Lifshitz transition and possible excitonic instability in ZrSiSe, Phys. Rev. Lett. **124**, 236601 (2020).

[41] X. Wang and J. Tan, Intrinsic anomalous Hall effect and lifshitz transition in a ferromagnetic kagome-lattice metal, Appl. Phys. Lett. **121**, 161903 (2022).

[42] O. Gunnarson, M. Calandra, and J. E. Han, *Colloquium*: Saturation of electrical resistivity, Rev. Mod. Phys. **75**, 1085 (2003).

[43] T. Jungwirth, Q. Niu, and A. H. MacDonald, Anomalous Hall effect in ferromagnetic semiconductors, Phys. Rev. Lett. **88**, 207208 (2002).

[44] M. Onoda and N. Nagaosa, Quantized anomalous Hall effect in two-dimensional ferromagnets: Quantum Hall effect in metals, Phys. Rev. Lett. **90**, 206601 (2003).

[45] P. Nozières and C. Lewiner, A simple theory of the anomalous Hall effect in semiconductors, J. Phys. France (Paris) **34**, 901 (1973).

[46] D. Xiao, M. C. Chang, and Q. Qiu, Berry phase effects on electronic properties, Rev. Mod. Phys. **82**, 1959 (2010).

[47] S. Onoda, N. Sugimoto, and N. Nagaosa, Quantum transport theory of anomalous electric, thermoelectric, and thermal Hall effects in ferromagnets, Phys. Rev. B **77**, 165103 (2008).

[48] P. N. Dheer, Galvanomagnetic effects in iron whiskers, Phys. Rev. **156**, 637 (1967).

[49] J. P. Jan and H. M. Gijsman, L'effet Hall du fer et du nickel aux basses températures, Physica **18**, 339 (1952).